Theoretical study on the electronic structures and phosphorescent properties of five bis-cyclometalated iridium(III) complexes with 2-phenylpyridinato ancillary ligand

ARTICLE *in* SYNTHETIC METALS · MAY 2014

Impact Factor: 2.25 · DOI: 10.1016/j.synthmet.2014.02.015

Synthetic Metals 191 (2014) 47–52

Contents lists available at ScienceDirect

Synthetic Metals

journal homepage: www.elsevier.com/locate/synmet

Theoretical study on the electronic structures and phosphorescent properties of five bis-cyclometalated iridium(III) complexes with 2-phenylpyridinato ancillary ligand

Deming Han [a], Qiang Zhang [a], Lihui Zhao [a], Gang Zhang [b], Qingshuang Wang [a,*]

[a] School of Life Science and Technology, Changchun University of Science and Technology, Changchun 130022, PR China
[b] State Key Laboratory of Theoretical and Computational Chemistry, Institute of Theoretical Chemistry, Jilin University, Changchun 130023, PR China

ARTICLE INFO

Article history:
Received 23 December 2013
Received in revised form 24 January 2014
Accepted 6 February 2014

Keywords:
DFT
TDDFT
Iridium
Phosphorescence

ABSTRACT

A DFT/TDDFT study was performed on five bis-cyclometalated iridium(III) complexes with the same ancillary ligand 2-phenylpyridinato (ppy) and main ligands with different substituted groups (—$CH(CH_3)_2$, —CH_3, —H, —F, and —NO_2). The geometry structures, electronic structures, absorption, and phosphorescent properties of the five iridium(III) complexes have been investigated. Calculations of ionization potential and electron affinity were used to evaluate the injection abilities of holes and electrons into these complexes. The lowest energy absorption wavelengths are located at 408 nm for **1**, 407 nm for **2**, 401 nm for **3**, 381 nm for **4**, and 556 nm for **5**, respectively, in good agreement with the HOMO–LUMO energy gaps. The lowest energy emissions of these complexes are localized at 515, 514, 516, 518, and 567 nm at M052X level, respectively. The calculated results indicate that the complex **4** possibly possesses the largest k_r value among the five complexes. We hope that this theoretical work can provide constructive information for designing and synthesizing novel phosphorescent materials for use in the organic light-emitting diodes.

1. Introduction

In the past two (plus) decades, organic light-emitting diodes (OLEDs) have attracted extensive attention since the tri(8-hydroxyquinolinato)aluminum(III) Alq_3 was used as an excellent electron-transport material or green fluorescence emitter [1]. In particular, phosphorescent transition-metal complexes (such as Ir(III), Re(I), Os(II), Ru(II), etc.) have been widely applied as materials in the light-emitting and the next generation material of the flat panel displays because both singlet and triplet excitons can be fully converted to light emission owing to the strong spin–orbit coupling of transition-metal ions [2–5]. Among them, cyclometalated iridium(III) complexes are known to be the promising candidates as OLED phosphors, which can display phosphorescent emission spanning the whole visible spectrum. Many homoleptic and heteroleptic cyclometalated iridium complexes have been theoretically studied, which are mostly based on the cyclometalating ligand 2-phenylpyridinato (ppy) with an ancillary ligand such as acetylacetonate (acac) or picolinate (pic) since the broad tunable emission-range was achieved for $Ir(ppy)_3$ by using chemical substitution tactics [6–10]. It is known that the introduction of electron-donating or electron-withdrawing substituents at different positions of the coordinated ligands is the most common approach to tune the emission energy [11–14]. Kim et al. have studied the photophysical, electrochemical, and electroluminescent (EL) properties of a series of highly efficient deep-blue phosphorescent Ir(III) complexes by the introduction of electron-donating and electron-withdrawing substituents on the ppy ligand [15]. Kang et al. have synthesized a blue phosphorescent iridium(III) complex bearing fluorine-substituted bipyridine (dfpypy) and investigated the effect of the substitution and replacement of the phenyl ring in ppy (phenylpyridine) with pyridine on the solid state structure and its photoluminescence [16].

Here, five Ir(III) complexes **1**, **2**, **3**, **4**, and **5** with the same ancillary ligand 2-phenylpyridinato (ppy) and main ligand with different substituted groups (—$CH(CH_3)_2$, —CH_3, —H, —F, and —NO_2) (Fig. 1a) have been investigated using the density functional theory (DFT) and time-dependent density functional theory (TDDFT). Comparison of electronic structures and spectral properties for the five complexes was carried out. These theoretical results are anticipated

* Corresponding author. Tel.: +86 431 85583023.
E-mail addresses: wangqingshuang2007@163.com, handeming2008@yahoo.com (Q. Wang).

http://dx.doi.org/10.1016/j.synthmet.2014.02.015
0379-6779/

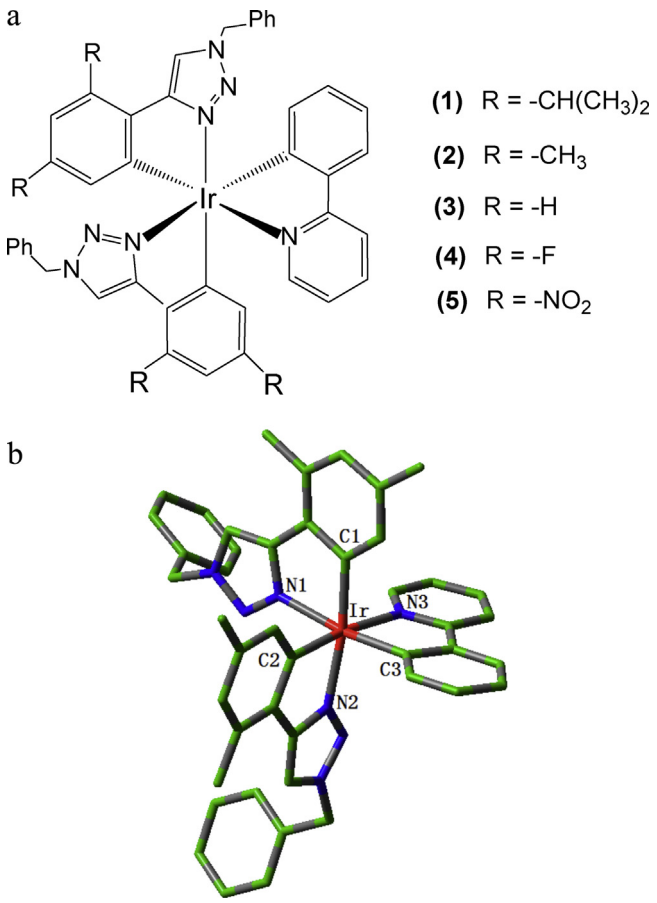

Fig. 1. (a) Sketch map of the structures of iridium(III) complexes **1**–**5** and (b) representative optimized structure of **2** (H atoms omitted).

to provide useful information of the optical and electronic properties of these complexes, and to present some guidelines for both fundamental research and practical applications in OLEDs in the future.

2. Computational details

The geometries of **1**–**5** in the ground and the excited states were optimized by the density functional theory (DFT) [17] method with Becke's three parameter hybrid method combined with the Lee–Yang–Parr correlation functional (denoted as B3LYP) [18,19]. On the basis of the optimized ground- and excited-state geometry structures, the time-dependent DFT (TDDFT) approach associated with the SCRF (self-consistent reaction field) theory using the integral equation formalism polarized continuum model (IEFPCM) [20] in dichloromethane (CH_2Cl_2) media was applied to simulate the absorption and emission spectral properties from the experimental results by Fernández-Hernández [21]. The "double-ξ" quality basis set LANL2DZ [22] associated with the pseudopotential was employed on atom Ir. The 6-31+G(d) basis set was used for non-metal atoms in the gradient optimizations. Furthermore, the stable configurations of these complexes can be confirmed by frequency analysis, in which no imaginary frequency was found for all configurations at the energy minima. In addition, the positive and negative ions with regard to the "electron-hole" creation are relevant to their use as OLEDs materials. Thus, ionization potentials (IP), electron affinities (EA), and reorganization energy (λ) were obtained by comparing the energy levels of neutral molecule with positive ions and negative ions, respectively. The calculated electronic density plots for frontier molecular orbitals were prepared by using the GaussView 5.0.8 software. The absorption spectra were simulated by using the GaussSum 2.5 [23] with the full width at half maximum (FWHM) of 3000 cm^{-1} based on the present TDDFT computational results. Recent calculations with the above-mentioned methods and basis sets for transition metal complexes have supported their reliability and gave good agreement with experimental results [24,25]. All calculations were performed with the Gaussian 09 software package [26].

3. Results and discussion

3.1. Geometries in the ground state S_0 and triplet excited state T_1

The schematic structures of the complexes **1**–**5** are presented in Fig. 1a, and the optimized ground state geometric structure for **2** is shown in Fig. 1b along with the numbering of some key atoms. The main geometric parameters in the ground and lowest triplet states are summarized in Table S1 (Supplementary information). These bis-cyclometalated complexes have the same ancillary ligand 2-phenylpyridinato (ppy) and different main ligands with substituted groups (—$CH(CH_3)_2$, —CH_3, —H, —F, and —NO_2). From the calculated results, it can be seen that all the optimized structures of these complexes are similar to each other, which presented the distorted octahedron structures. As shown in Table S1, compared with **3**, the Ir—C3 and Ir—N3 bond lengths of **1** and **2** with electron-donating substituent at the main ligands is relaxed. The Ir—C3 and Ir—N3 bond lengths of **4** and **5** with electron-withdrawing substituent at the main ligand are relaxed and tighten, respectively. The dihedral angles C1—N1—N2—C3 and N1—C2—C3—N3 of **1**–**5** are mostly less than 10°.

On the whole, for the triplet excited state T_1, the bond distances are shorter for Ir—C1 and Ir—C3 bonds and longer for Ir—C2 bonds compared with those in the singlet state (S_0). Meanwhile, the bond angle C3—Ir—N1 is slightly larger compared with the ground state one. In addition, the dihedral angles of C1—Ir—C3—N3 in T_1 state are smaller than those in S_0 state for complexes **1**–**4**. In contrast, the dihedral angles of N1—C2—C3—N3 in T_1 state for the five complexes are obviously larger than those in S_0 state.

3.2. Molecular orbital properties

The properties of the excited states and electronic transitions of organic light-emitting materials are known to be closely related to the characters of the frontier molecular orbitals (FMOs), especially HOMO (highest occupied molecular orbital) and LUMO (lowest unoccupied molecular orbital). The HOMO and LUMO distribution, energy levels, and energy gaps between of LUMO and HOMO ($\Delta E_{L\rightarrow H}$) of the five complexes **1**–**5** are plotted in Fig. 2. The calculated FMOs compositions for **1**–**5** were listed in Tables S2–S6 (Supplementary information).

Fig. 2 and Tables S2–S6 show that for **1**, **2**, **4**, and **5**, the HOMO have the similar distribution with Ir d-orbital and ancillary ligands; however, for **3**, the HOMO has the distribution on all the complex. For LUMO of **1**–**4**, there are main distributions on the ancillary ligands. However, it is different that the LUMO of **5** has 99% compositions from the main ligands, which can also be seen from Table S6 and Fig. 2. For **1** and **2**, the energies of HOMO and LUMO are slightly different due to the different substituted groups on main ligands, i.e., HOMO – 4.57 eV and LUMO – 0.84 eV in **1**, HOMO – 4.56 eV, LUMO – 0.82 eV in **2**, and the HOMO–LUMO energy gaps ($\Delta E_{L\rightarrow H}$) are nearly the same, i.e., 3.73 eV for **1**, 3.74 eV for **2**. This indicates that the change of substituted groups on main ligands from —$CH(CH_3)_2$ in **1** to —CH_3 in **2** affects slightly the energy levels and the $\Delta E_{L\rightarrow H}$. Compared to **3**, the **4** and **5** with the electron-withdrawing group —F and —NO_2 located at the main ligand has

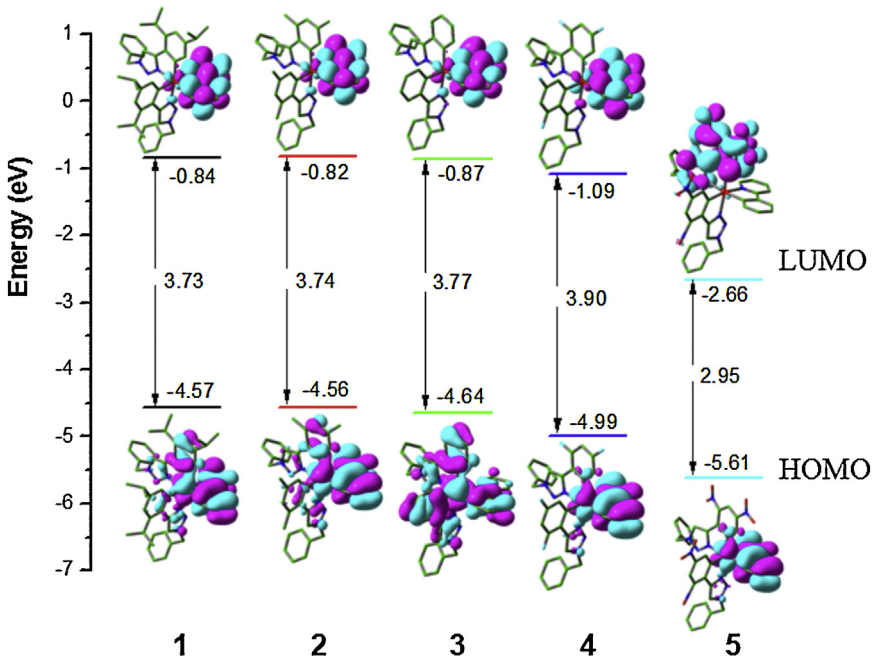

Fig. 2. Molecular orbital diagrams and HOMO and LUMO energies for complexes **1**–**5**.

Table 1
The calculated vertical IP (IP_v), adiabatic IP (IP_a), hole extraction potential (HEP), vertical EA (EA_v), and adiabatic EA (EA_a), electron extraction potential (EEP), and reorganization energies for electron ($\lambda_{electron}$) and hole (λ_{hole}), unit: eV.

	IP_v	IP_a	HEP	EA_v	EA_a	EEP	$\lambda_{electron}$	λ_{hole}
1	5.611	5.522	5.399	0.240	0.169	0.103	0.136	0.212
2	5.641	5.542	5.424	0.269	0.197	0.128	0.140	0.217
3	5.763	5.673	5.569	0.246	0.173	0.107	0.138	0.193
4	6.130	6.015	5.864	0.078	0.007	0.063	0.142	0.266
5	6.756	6.590	6.394	1.511	1.652	1.783	0.272	0.362

lower HOMO and LUMO energies. However, **4** and **5** have the largest and smallest $\Delta E_{L\rightarrow H}$ values (3.90 and 2.95 eV, respectively) among the five complexes.

3.3. Comparison of performance in OLEDs

The ionization potential (IP), electron affinity (EA), reorganization energy (λ), hole extraction potential (HEP), and electron extraction potential (EEP) for the complexes **1**–**5** have been calculated to understand the charge injection and transporting properties of luminescent materials (Table 1). In addition, the IP_v is defined as the energy difference between the cation and its neutral molecule at the equilibrium geometry of the neutral molecule. The IP_a is defined as the energy difference between the cation and its neutral molecule at their own equilibrium geometries. The EA_v is defined as the energy difference between the neutral molecule and its anion both at the equilibrium geometry of the anion. The EA_a is defined as the energy difference between the neutral molecule and its anion at their own equilibrium geometries. In Table 1, the IP value of complex **1** is the smallest one, which means that the hole injection is much easier in complex **1** than others. It can be seen that the IP values increased from **1** to **5** with the larger electron-withdrawing ability of substituted groups on main ligands. The EA value of complex **5** is the largest, which means the electron injection is much easier than the other complexes.

According to the Marcus–Hush model [27–29], the charge (hole or electron) transfer rate K_{et} can be expressed by the following formula:

$$K_{et} = A \exp\left(\frac{-\lambda}{4k_B T}\right) \quad (1)$$

where T is the temperature, k_B is the Boltzmann constant, λ is the reorganization energy. Due to the limited intermolecular charge transfer range in the solid state, the mobility of charges has been demonstrated to be predominantly related to the internal reorganization energy λ for OLEDs materials [30–33]. Generally, λ is determined by fast changes in molecular geometry (the internal reorganization energy λ_i) and by slow variations in solvent polarization of the surrounding medium (the external reorganization energy λ_e). In OLEDs devices, the contribution from λ_e can be neglected. Therefore, the internal reorganization energy λ_i is the determinant factor. λ_i for hole transfer (λ_{hole}) can be expressed as follows [34]:

$$\lambda_{hole} = \lambda_0 + \lambda_+ = (E_0^+ - E_0) + (E_+^* - E_+) = IP_v - HEP \quad (2)$$

as illustrated in Fig. 3, E_0 and E_+ represent the energies of the neutral and cationic species in their lowest energy geometries, respectively, while E_0^* and E_+^* represent the energies of the neutral and cationic species with the geometries of the cationic and neutral species, respectively, which is equal to the difference between IP_v and HEP. Similarly, the reorganization energy for electron transport ($\lambda_{electron}$) can be evaluated as: $\lambda_{electron} = EEP - EA_v$. As emitting layer materials, it needs to achieve hole and electron injection and transport balance. To the best of our knowledge, the reorganization energy (λ) can be approximately used to estimate the charge transport rate and balance between holes and electrons. The results are also listed in Table 1. The reorganization energies for hole transport (λ_{hole}) are obviously larger than electron transport ($\lambda_{electron}$), which indicates that electron transport has better performance than hole transport. In addition, one can find that complex **3** has the best hole transfer ability with the smallest λ_{hole} value (0.193 eV) among the five complexes. We also found that the energy differences between λ_{hole} and $\lambda_{electron}$ for **1**–**5** are 0.076, 0.077, 0.055, 0.124, and 0.090 eV, respectively. It can be seen that **1** and **3** with the smaller λ value and the smaller differences between λ_{hole} and

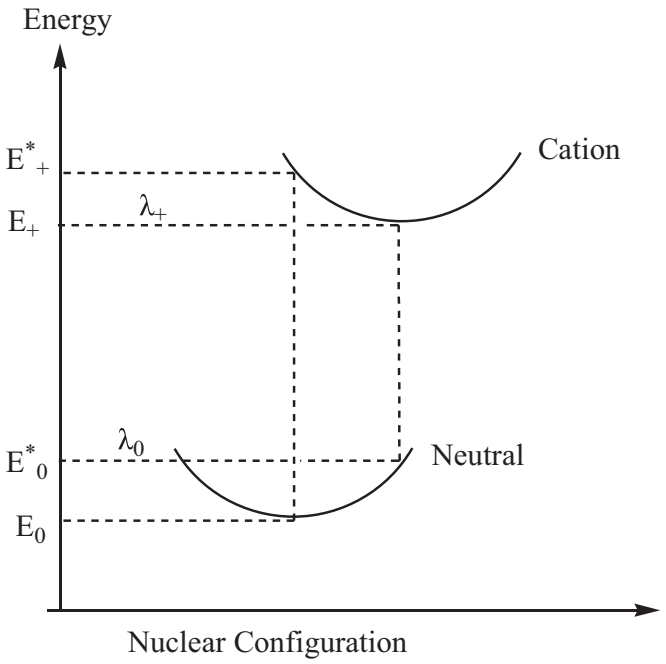

Fig. 3. Schematic description of the internal reorganization energy for hole transfer.

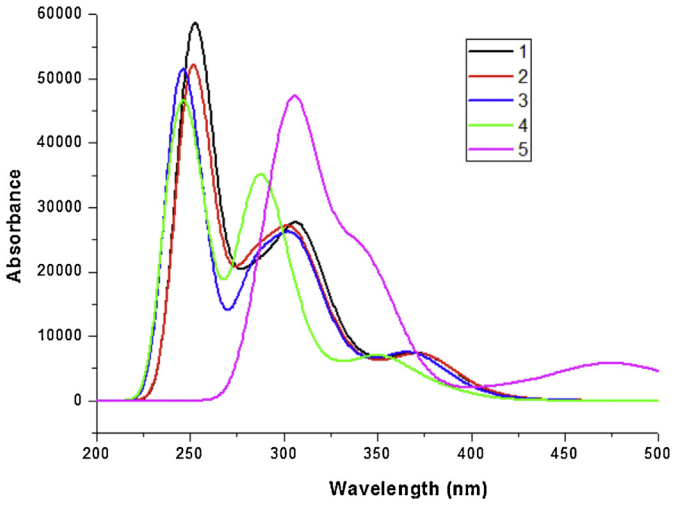

Fig. 4. Simulated absorption spectra in CH_2Cl_2 for **1**–**5**.

$\lambda_{electron}$ indicates the better transfer balance between holes and electrons. As shown in Table 1, the λ_{hole} values for **1**–**5** are larger than the $\lambda_{electron}$ values, which suggests that the electron transfer rate is better than the hole transfer rate. While the difference between $\lambda_{electron}$ and λ_{hole} for **1**, **2**, **3**, and **5** are much smaller than that of complex **4**, which can greatly improve the charge transfer balance, thus further enhancing the device performance of OLEDs. The above analysis indicates that the charge transfer rate of holes and electrons has been obviously influenced by the electron-withdrawing and electron-donating substituted groups on main ligands.

3.4. Absorption spectra

On the basis of the optimized ground state geometries, the absorption properties of **1**–**5** were calculated using TDDFT method. The vertical electronic excitation energies, oscillator strengths (*f*), assignment, and configurations have been listed in Table S7 (Supplementary information). The absorption spectra of the studied complexes in CH_2Cl_2 media based on the TDDFT calculations are shown in Fig. 4.

The calculated lowest energy absorption wavelengths are located at 408 nm (f = 0.0037) for **1**, 407 nm (f = 0.0045) for **2**, 401 nm (f = 0.0072) for **3**, 381 nm (f = 0.0199) for **4**, and 556 nm (f = 0.0040) for **5**, respectively, in good agreement with the energy gaps ($\Delta E_{L\rightarrow H}$) trend (Fig. 2) because the HOMO–LUMO transition configurations are predominantly responsible for the $S_0 \rightarrow S_1$ transition (**1**: 95%; **2**: 95%; **3**: 97%; **4**: 96%; **5**: 97%). It can be seen that the calculated 381 nm absorption for **4** is in good agreement with the experimental value 387 nm [21]. As seen in Fig. 4, complexes **1**–**4** have similar absorption curves. Besides, **5** has the different absorption peak at strong absorption at the about 305 nm, a large peak appearing. For **1**–**5**, the lowest lying transition are attributed to the HOMO → LUMO transition with MLCT (metal to ligand charge transfer)/LLCT(ligand to ligand charge transfer). The assignment of the lowest lying absorption for **1**, **2**, and **4** can be described as the $d(Ir)+\pi(A)\rightarrow\pi^*(B)$ transition. Besides, for **3** and **5**, the lowest energy absorption are attributed to the $d(Ir)+\pi(A+B)\rightarrow\pi^*(B)$ and $d(Ir)+\pi(B)\rightarrow\pi^*(A)$ transitions, which is seen from the HOMO and LUMO electronic density contour in Fig. 2.

3.5. Phosphorescence

On the basis of the optimized T_1 structures, the emission wavelengths, emission energies, and transition nature of complexes **1**–**5** calculated by the TDDFT method in CH_2Cl_2 solution have been listed in Table 2. To check the computational method, two different density functionals (B3LYP and M052X [35]) were used. A good agreement with experimental data was obtained for M052X, while a disagreement was found for B3LYP. The calculated lowest energy emissions for **1**–**5** at M052X level are localized at 515, 514, 516, 518, and 567 nm, vs. 564, 564, 564, 559, and 745 nm at B3LYP level. For **4**, the lowest energy emission at M052X (518 nm) is in good agreement with the experimental value (510 nm) vs. the significant deviation of 49 nm at B3LYP level from the experimental data [21].

It can be seen that complexes **1**–**3** have the similar lowest energy emissions, indicating that electron-donating substituted groups on main ligands have no obvious effect on the emission properties. With respect to **3**, the lowest energy emission of **5** is located at 567 nm due to the strong electron-withdrawing substituted group

Table 2
Phosphorescent emissions of **1**–**5** in CH_2Cl_2 medium at the TDDFT/B3LYP and TDDFT/M052X levels, respectively, along with experimental wavelength (nm) available.

	B3LYP		M052X		Nature	Exptl.[a]
	λ (nm)	Configuration	λ (nm)	Configuration		
1	564	L → H (71%)	515	L → H (71%)	^{3}MLCT/^{3}LLCT	
2	564	L → H (73%)	514	L → H (73%)	^{3}MLCT/^{3}LLCT	
3	564	L → H (78%)	516	L → H (77%)	^{3}MLCT/^{3}LLCT	
4	559	L → H (83%)	518	L → H (82%)	^{3}MLCT/^{3}LLCT	510
5	745	L → H-1 (72%)	567	L → H-1 (72%)	^{3}MLCT/^{3}LLCT	

[a] From Ref. [21].

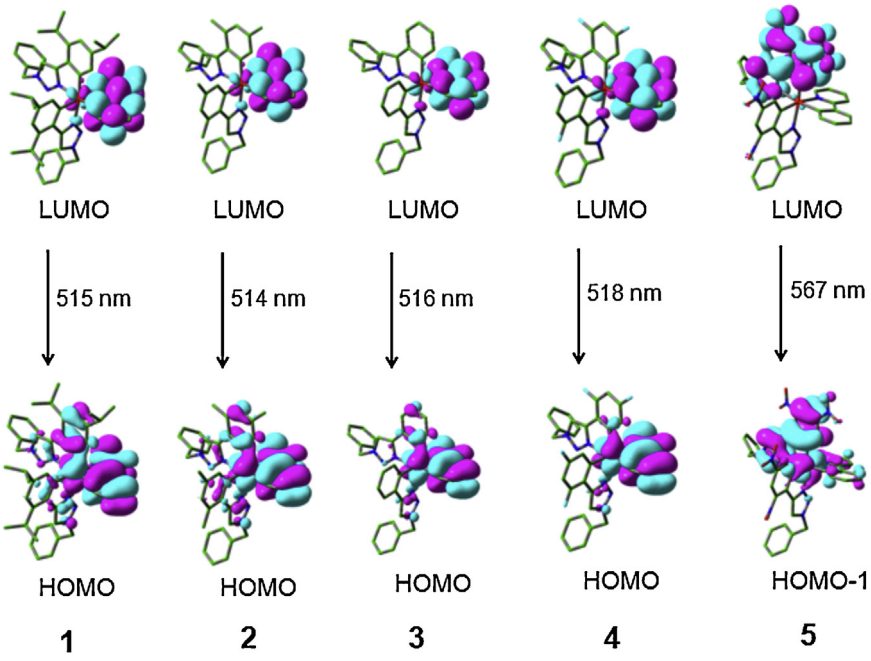

Fig. 5. Transitions responsible for the emissions at 515, 514, 516, 518, and 567 nm for complexes **1**–**5**, respectively, simulated in CH_2Cl_2 media at M052X level.

(—NO_2) on main ligands. For **1**–**5**, its emission transition character is assigned to ^{3}MLCT/^{3}LLCT (ligand to ligand charge transfer). From Fig. 5, it can be seen that the complexes **1**–**4** have the similar HOMO and LUMO distributions. Specifically, the LUMO is mainly localized at the ancillary ligand; the HOMO is mainly localized at the auxiliary ligand and the central metal atom iridium. However, complex **5** has the different lowest-lying triplet transition nature LUMO → HOMO − 1. In addition, the HOMO − 1 and LUMO distribution for **5** is also obviously different in contrast to that of 1–**4**, which can be due to the strong electron-withdrawing group —NO_2 at the main ligand.

3.6. Phosphorescence quantum efficiency

The emission quantum yield (Φ) can be affected by the competition between k_r (radiative decay rate) and k_{nr} (nonradiative decay rate), i.e., $\Phi = k_r/(k_r + k_{nr})$. It can be seen, to increase the quantum yield, k_r should be increased and k_{nr} should be decreased simultaneously or respectively [36,37]. In addition, k_r is also theoretically related to the mixing between S_1 and T_1, which is proportional to the spin–orbit coupling (SOC) and inversely proportional to the energy gaps between the S_1 and T_1 states according to the following formula [38,39]:

$$k_r \approx \gamma \frac{\left\langle \psi_{S_1} \left| H_{S_0} \right| \psi_{T_1} \right\rangle^2 \mu_{S_1}^2}{\left(\Delta E_{S_1-T_1}\right)^2} \qquad (3)$$

$$\gamma = 16\pi^3 10^6 n^3 E_{em}{}^3/3h\varepsilon_0$$

where H_{S_0} is the Hamiltonian for the spin–orbit coupling, μ_{S_1} is the transition dipole moment in the $S_0 \rightarrow S_1$ transition, $\Delta E_{S_1-T_1}$ is the energy gaps between the S_1 and T_1 states, E_{em} represents the emission energy in cm^{-1} and n, h, and ε_0 are the refractive index, Planck's constant and the permittivity in a vacuum, respectively. Accordingly, the variation of quantum yield (Φ) can be qualitatively analyzed in theory from the above formula.

The heavy atom participation is believed to increase the spin–orbit coupling (SOC) effects and intersystem crossing (ISC), which its orbitals make a significant contribution on the excited states involved. It is known that the phosphorescence quantum efficiencies could be increased by a larger contribution of MLCT in the T_1 state. For iridium atom, the direct involvement of the d(Ir) orbital enhances the first-order SOC in the $T_1 \rightarrow S_0$ transition and thus ISC, which would result in a drastic decrease of the radiative lifetime and avoid the nonradiative process [40]. In Table 2, we have listed the ^{3}MLCT contributions which were calculated to be 31.2%, 31.3%, 34.6%, 29.9% and 37.4% for **1**, **2**, **3**, **4**, and **5**, respectively. It is also known that the phosphorescence quantum efficiencies are inversely proportional to the $\Delta E_{S_1-T_1}$ [25]. Namely, a minimal $\Delta E_{S_1-T_1}$ is required for enhancing the ISC rate, leading to the increased k_r. In addition, the phosphorescence quantum efficiencies are proportional to the μ_{S_1} values. The $\Delta E_{S_1-T_1}$ values for these complexes are listed in Table 3, along with the μ_{S_1} values. The results give 0.04, 0.06, 0.09, 0.25 and 0.07 eV for the $\Delta E_{S_1-T_1}$, respectively for **1**, **2**, **3**, **4**, and **5**. The μ_{S_1} values are 0.04, 0.06, 0.09, 0.25 and 0.07 Debye, respectively for **1**, **2**, **3**, **4**, and **5**. From the discussion above, it is obvious that a lower $\Delta E_{S_1-T_1}$ and larger ^{3}MLCT contributions and higher μ_{S_1} values may account for a larger k_r according to Eq. (3). From the data in Table 3, it can be seen that the complex **4** has possibly the largest k_r value among these complexes.

Table 3
The contribution of ^{3}MLCT (%) in the T_1 state and the energy gaps between the S_1 and T_1 states ($\Delta E_{S_1-T_1}$) (in eV), along with the transition electric dipole moment in the $S_0 \rightarrow S_1$ transition μ_{S_1} (Debye), the radiative decay rate k_r ($\times 10^5\ s^{-1}$) and nonradiative decay rate k_{nr} ($\times 10^5\ s^{-1}$), together with the measured lifetime τ (μs) and quantum yields Φ (%) for the studied complex **4** in CH_2Cl_2 solution.

	^{3}MLCT	$\Delta E_{S_1-T_1}$	μ_{S_1}	Φ[a]	τ[a]	k_r[a]	k_{nr}[a]
1	31.2	0.49	0.04				
2	31.3	0.50	0.06				
3	34.6	0.53	0.09				
4	29.9	0.66	0.25	0.76	2.6	2.9	0.9
5	37.4	0.35	0.07				

[a] Ref. [21].

4. Conclusions

In this paper, we have applied DFT and TDDFT methods to study the geometries, electronic structures, injection and transporting, absorption and phosphorescence properties of five

bis-cyclometalated iridium(III) complexes with the same ancillary ligand 2-phenylpyridinato (ppy) and different main ligands with substituted groups (—$CH(CH_3)_2$, —CH_3, —H, —F, and —NO_2). Meanwhile, we also investigate the influence of different substituted groups at main ligands on the properties of these complexes. The molecular orbitals have been investigated to study the microcosmic charge transfer transitions in absorption and emission. Ionization potential (IP), electron affinities (EA) and reorganization energy were obtained to evaluate the charge transfer and balance properties between hole and electron. The calculated absorption and phosphorescent properties of the five complexes are compared with the available experimental data and a good agreement is obtained. These theoretical studies could provide some useful information in designing new phosphorescent materials for OLEDs applications.

Acknowledgments

The authors are grateful to the financial aid from the Program of Science and Technology Development Plan of Jilin Province (Grant Nos. 20130203032YY, 20140520090JH) and the Funds for Doctoral Scientific Research Startup of Changchun University of Science and Technology (Grant No. 40301855).

Appendix A. Supplementary data

Supplementary material related to this article can be found, in the online version, at http://dx.doi.org/10.1016/j.synthmet.2014.02.015.

References

[1] C.W. Tang, S.A. VanSlyke, Appl. Phys. Lett. 51 (1987) 913–915.
[2] U. Mitschle, P.J. Bäuerle, J. Mater. Chem. 10 (2000) 1471–1507.
[3] M.A. Baldo, M.E. Thompson, S.R. Forrest, Nature 403 (2000) 750–753.
[4] Y. Sun, N.C. Giebink, H. Kanno, B. Ma, M.E. Thompson, S.R. Forrest, Nature 440 (2006) 908–912.
[5] X.H. Shang, D.M. Han, D.F. Li, Z.J. Wu, Chem. Phys. Lett. 565 (2013) 12–17.
[6] E. Baranoff, H.J. Bolink, F. De Angelis, S. Fantacci, D. Di Censo, K. Djellab, M. Gratzel, K. Nazeeruddin, Dalton Trans. 39 (2010) 8914–8918.
[7] E. Baranoff, B.F.E. Curchod, J. Frey, R. Scopelliti, F. Kessler, I. Tavernelli, U. Rothlisberger, M. Gratzel, K. Nazeeruddin, Inorg. Chem. 51 (2012) 215–224.
[8] M.S. Lowry, W.R. Hudson, R.A. Pascal, S. Bernhard, J. Am. Chem. Soc. 126 (2004) 14129–14135.
[9] E. Holder, B.M.W. Langeveld, U.S. Schubert, Adv. Mater. 17 (2005) 1109–1121.
[10] A. Beeby, S. Bettington, I.D.W. Samuel, Z.J. Wang, J. Mater. Chem. 13 (2003) 80–83.
[11] C.S.K. Mak, A. Hayer, S.I. Pascu, S.E. Watkins, A.B. Holmes, A. Köhler, R.H. Friend, Chem. Commun. (2005) 4708–4710.
[12] F.M. Hwang, H.Y. Chen, P.S. Chen, C.S. Liu, Y. Chi, C.F. Shu, F.I. Wu, P.T. Chou, S.M. Peng, G.H. Lee, Inorg. Chem. 44 (2005) 1344–1353.
[13] C.H. Yang, S.W. Li, Y. Chi, Y.M. Cheng, Y.S. Yeh, P.T. Chou, G.H. Lee, C.H. Wang, C.F. Shu, Inorg. Chem. 44 (2005) 7770–7780.
[14] T.H. Kwon, H.S. Cho, M.K. Kim, J.W. Kim, J.J. Kim, K.H. Lee, S.J. Park, I.S. Shin, H. Kim, D.M. Shin, Y.K. Chung, J.I. Hong, Organometallics 24 (2005) 1578–1585.
[15] H.J. Seo, K.M. Yoo, M. Song, J.S. Park, S.H. Jin, Y.I. Kim, J.J. Kim, Org. Electron. 11 (2010) 564–572.
[16] S.J. Lee, K.M. Park, K. Yang, Y. Kang, Inorg. Chem. 48 (2009) 1030–1037.
[17] A.D. Becke, J. Chem. Phys. 98 (1993) 5648–5652.
[18] C. Lee, W.T. Yang, R.G. Parr, Phys. Rev. B 37 (1988) 785–789.
[19] P.J. Hay, W.R. Wadt, J. Chem. Phys. 82 (1985) 270–284.
[20] E. Cances, B. Mennucci, J. Tomasi, J. Chem. Phys. 107 (1997) 3032–3042.
[21] J.M. Fernández-Hernández, J.I. Beltrán, V. Lemaur, M.D. Gálvez-López, C.H. Chien, F. Polo, E. Orselli, R. Frohlich, J. Cornil, Luisa De Cola, Inorg. Chem. 52 (2013) 1812–1824.
[22] P.J. Hay, W.R. Wadt, J. Chem. Phys. 82 (1985) 299–310.
[23] N.M. O'Boyle, A.L. Tenderholt, K.M. Langner, J. Comput. Chem. 29 (2008) 839–845.
[24] I. Avilov, P. Minoofar, J. Cornil, L. De Cola, J. Am. Chem. Soc. 129 (2007) 8247–8258.
[25] L.L. Shi, Y. Geng, H.Z. Gao, Z.M. Su, Z.J. Wu, Dalton Trans. 39 (2010) 7733–7740.
[26] M.J. Frisch, G.W. Trucks, H.B. Schlegel, G.E. Scuseria, M.A. Robb, J.R. Cheeseman, G. Scalmani, V. Barone, B. Mennucci, G.A. Petersson, H. Nakatsuji, M. Caricato, X. Li, H.P. Hratchian, A.F. Izmaylov, J. Bloino, G. Zheng, J.L. Sonnenberg, M. Hada, M. Ehara, K. Toyota, R. Fukuda, J. Hasegawa, M. Ishida, T. Nakajima, Y. Honda, O. Kitao, H. Nakai, T. Vreven, J.A. Montgomery Jr., J.E. Peralta, F. Ogliaro, M. Bearpark, J.J. Heyd, E. Brothers, K.N. Kudin, V.N. Staroverov, R. Kobayashi, J. Normand, K. Raghavachari, A. Rendell, J.C. Burant, S.S. Iyengar, J. Tomasi, M. Cossi, N. Rega, J.M. Millam, M. Klene, J.E. Knox, J.B. Cross, V. Bakken, C. Adamo, J. Jaramillo, R. Gomperts, R.E. Stratmann, O. Yazyev, A.J. Austin, R. Cammi, C. Pomelli, J.W. Ochterski, R.L. Martin, K. Morokuma, V.G. Zakrzewski, G.A. Voth, P. Salvador, J.J. Dannenberg, S. Dapprich, A.D. Daniels, J.B. Foresman, J.V. Ortiz, J. Cioslowski, D.J. Fox, Gaussian 09, Gaussian Inc., Wallingford, CT, 2009.
[27] N.S. Hush, J. Chem. Phys. 28 (1958) 962–972.
[28] R.A. Marcus, Rev. Mod. Phys. 65 (1993) 599–610.
[29] R.A. Marcus, J. Chem. Phys. 24 (1956) 966–978.
[30] M. Malagoli, J.L. Brédas, Chem. Phys. Lett. 327 (2000) 13–17.
[31] B.C. Lin, C.P. Cheng, Z. Ping, M. Lao, J. Phys. Chem. A 107 (2003) 5241–5251.
[32] K. Sakanoue, M. Motoda, M. Sugimoto, S. Sakaki, J. Phys. Chem. A 103 (1999) 5551–5556.
[33] Y.Z. Lee, X.W. Chen, S.A. Chen, P.K. Wei, W.S. Fann, J. Am. Chem. Soc. 123 (2001) 2296–2307.
[34] G.R. Hutchison, M.A. Ratner, T.J. Marks, J. Am. Chem. Soc. 127 (2005) 2339–2350.
[35] Y. Zhao, N.E. Schultz, D.G. Truhlar, J. Chem. Theory Comput. 2 (2006) 364–382.
[36] S. Fantacci, F. De Angelis, A. Sgamellotti, A. Marrone, N. Re, J. Am. Chem. Soc. 127 (2005) 14144–14145.
[37] A.B. Tamayo, S. Garon, T. Sajoto, P.I. Djurovich, I.M. Tsyba, R. Bau, M.E. Thompson, Inorg. Chem. 44 (2005) 8723–8732.
[38] S. Haneder, E. Da Como, J. Feldmann, J.M. Lupton, C. Lennartz, P. Erk, E. Fuchs, O. Molt, I. Munster, C. Schildknecht, G. Wagenblast, Adv. Mater. 20 (2008) 3325–3330.
[39] N. Turro, Modern Molecular Photochemistry, University Science Books, Palo Alto, USA, 1991.
[40] C.H. Yang, Y.M. Cheng, Y. Chi, C.J. Hsu, F.C. Fang, K.T. Wong, P.T. Chou, C.H. Chang, M.H. Tsai, C.C. Wu, Angew. Chem. Int. Ed. 46 (2007) 2418–2421.